Journal of Power Sources 189 (2009) 297–302

Contents lists available at ScienceDirect

Journal of Power Sources

journal homepage: www.elsevier.com/locate/jpowsour

Electrospraying-assisted synthesis of tin nanoparticles for Li-ion battery electrodes

M. Valvo*, U. Lafont, D. Munao, E.M. Kelder

NanoStructured Materials, Delft Research Centre for Sustainable Energy, Delft University of Technology, Julianalaan 136, 2628 BL Delft, The Netherlands

ARTICLE INFO

Article history:
Received 31 July 2008
Accepted 8 September 2008
Available online 18 September 2008

Keywords:
Electrospraying
Reductive precipitation
Li–Sn alloys
Sn oxides
Li-ion batteries

ABSTRACT

Reductive precipitation of Sn(II) chloride by $NaBH_4$ is assisted by electrospraying in order to achieve a fine dispersion of the liquid precursor solution into the reductive bath. The formation of a highly charged aerosol of precursor droplets enables the size reduction of the constitutive units for the synthesized materials. Nanostructured Sn-based powders resulting from this process are tested as negative electrodes in Li cells. The presence of nanostructures has a significant influence on the cycling behaviour of the materials, which retained a capacity of about 300 mAh g^{-1} after 100 cycles measured between 0.05 and 1.20 V.

1. Introduction

Sn and Sn-based composites are interesting materials for advanced Li-ion batteries negative electrodes. The reversible reaction of metal Sn with Li ions yields gravimetric capacities as high as 993 mAh g^{-1}, which outperform those of commercial electrodes based on carbonaceous materials (i.e. 372 mAh g^{-1} for graphite). Moreover, the formation of lithium–tin alloys is associated with electrochemical potentials versus Li/Li^+ that are considerably higher than that of lithiated graphite [1,2]. This situation is favourable for practical purposes, since it improves the safety which is related to the reactivity of the host and the possibility of depositing metallic lithium [3]. Although these attractive features have initiated a number of studies on Sn-based hosts [1–8] as alternative negative electrodes for Li cells, a major drawback has hindered their use for practical applications in rechargeable Li-ion batteries. A severe volume change of the host material (i.e. up to about 250% with respect to the unstrained β-Sn lattice) during uptake and removal of Li ions is responsible for extended cracking and pulverization of these electrodes upon repeated cycling. In particular, bulk and coarse-grained Sn materials undergo loss of electrical contact with the current collector after few cycles, leading to early failure of the cell [7]. In this respect, the use of Sn-based nanoparticles and nanocomposites offers an effective way to enhance the mechanical stability of these materials upon prolonged cycling. On the one hand, employing reactive phases finely dispersed in less-active or inert phases – as in multiphases or composite electrodes – has the beneficial effect of buffering the volume changes during electrochemical cycling, and alleviating the stresses arising from this process [5]. On the other hand, reducing the size of the host particles results in a better acceptance of the induced local strain and it also favours the reaction kinetics, due to shorter migration lengths for lithium.

Nevertheless, decreasing the size of the primary particles to few nanometres, while retaining a homogeneous size distribution, still seems to be a crucial issue for most of the synthesis methods applied so far. For example, high-energy ball milling and reductive precipitation are easy techniques that have been extensively employed for the synthesis of metallic, intermetallic and alloyed Sn fine powders [7,9–12]. These methods have advantages and drawbacks that are characteristic for the type of the approach used (i.e. top–down versus bottom–up) and for the environment in which the process is carried out (i.e. dry versus wet).

Reductive precipitation of Sn chlorides by $NaBH_4$ constitutes an interesting alternative to mechanic-milling, since its bottom–up approach should provide an easier route to nanoparticles formation. Despite that, in most of the cases, small nanoparticles with homogeneous size distribution cannot be directly achieved via this simple reduction process [12,13]. Therefore, the use of suitable surfactants or capping agents during the synthesis becomes a prerequisite [13].

* Corresponding author. Tel.: +31 15 2785536; fax: +31 15 2784945.
E-mail address: m.valvo@tudelft.nl (M. Valvo).

0378-7753/$ – see front matter © 2008 Elsevier B.V. All rights reserved.
doi:10.1016/j.jpowsour.2008.09.019

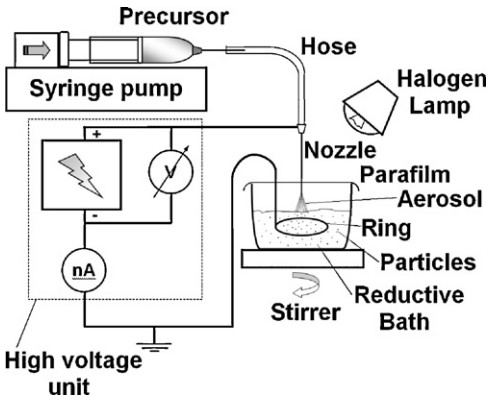

Fig. 1. Schematic drawing of the setup for EHDA-assisted synthesis.

Recently, an advanced method for carrying out reductive precipitation of metal chlorides by $NaBH_4$ has been proposed [14]. The concept underlying this technique is the use of an electrospray for atomizing the liquid precursors in the form of charged aerosols. Electrospraying, which is also more precisely referred to as electrohydrodynamic atomization (EHDA), is a powerful technique which uses high electric fields for dispersing liquids. Nowadays this method is being increasingly applied to modern materials technologies and to nanotechnology [15–17]. Herein, electrospray provides a top–down approach, through which the size of the droplets containing the metal precursors can be typically reduced to a few microns or less, prior to their contact with the reductive agent. In this way, a discontinuous dripping of the liquid precursors (i.e. drop-wise addition) can be easily converted into a continuous flow of highly charged droplets or micro-jets, in order to achieve a higher dispersion into the reductive bath. The atomization step adds a complementary control on the standard chemical synthesis, because the precursor droplet size, their velocity, acceleration, evaporation and charge can be influenced to a certain extent by adjusting the EHDA parameters.

In this study, we present our current investigations on nanostructured powders that have been obtained via electrospraying-assisted precipitation of Sn(II) chloride, and their electrochemical behaviour in Li cells. Electrochemical cycling of these materials is compared to that of commercial Sn powders that were taken here as reference.

2. Experimental

Tin nanoparticles were synthesized by electrospraying a Sn precursor (0.1 M solution of $SnCl_2{\cdot}2H_2O$ in isopropyl alcohol – IPA) into a reductive bath, where $NaBH_4$ was used as reductive agent in IPA. The precursor solution was pumped at a constant flow rate of 3.5 ml h^{-1} through an electrified capillary. Different voltages, i.e. ~3 and ~9 kV, were applied between a stainless nozzle and a ring made of Sn soldering wire, which was dipped in the reductive bath, in order to achieve EHDA in the so-called "cone-jet" and "multi-jet" modes, respectively [18]. A schematic drawing of the experimental setup is depicted in Fig. 1.

Powder production and collection were carried out in air at room temperature (RT) following a procedure similar to the one described previously [14]. Different techniques were employed to investigate the crystallinity, the morphology and the structure of the produced powders. In that regard, X-rays diffraction (XRD) was performed on a Bruker (AXS D8 Advance) X-ray diffractometer with a Cu Kα radiation source (λ = 1.5418 Å) between 10° and 85°. Transmission electron microscopy (TEM) and scanning electron microscopy (SEM) were carried out on a Philips CM30T Transmission Electron Microscope operated at 300 kV and a Philips XL20 Scanning Electron Microscope, respectively. Further imaging of the produced materials was carried out via atomic force microscopy (AFM) on a NT-MDT NTEGRA Scanning Probe Microscope in semi-contact mode, using a micro-fabricated Si cantilever and tip (NT-MDT, Silicon: NSG 03).

Electrochemical measurements were performed on CR2320-type coin cells assembled in a He-filled glove box. Composite electrodes were prepared by casting a slurry of dry active powders with carbon black (CB) and polyvinylidene fluoride (PVdF) in a 3:1:1 weight ratio in *N*-methylpyrrolidone (NMP) onto a thin copper foil (Akashi – 0.018 mm), followed by drying in a convection oven around 100°. Before usage, the electrodes were roller-pressed and circular disks of 14 mm diameter were punched out and weighed. The coated electrodes were dried under vacuum before assembling in coin cells, having metallic lithium as reference and counter electrode and a 1 M $LiPF_6$ solution in EC:DMC (2:1, w/w) as electrolyte. The cells were discharged and charged in different voltage ranges versus Li/Li^+. Galvanostatic tests were performed with a Maccor (S-4000) cycler at a constant gravimetric current density of 113 mA g^{-1}. Only in one case, the first cycle was carried out at a lower current density of 23 mA g^{-1}.

3. Results and discussion

The materials produced via this process, hereafter referred to as electrostatic spray reductive precipitation (ESRP) for simplicity, were analysed by XRD. The results are shown in Fig. 2, where micrometric Sn powders (Aldrich, −325 mesh) are included as reference material.

Employing a high voltage has a clear influence on the diffraction pattern of the produced materials. The applied electric field is effective in reducing the size of the materials, as indicated by an increased broadening of the characteristic diffraction peaks when compared to those of the commercial powders. In particular, the most intense peaks in Fig. 2(b) match with the characteristic reflections of the β-Sn lattice structure (JCPDS No. 04-0673). No crystalline impurities related to reaction by-products or to crystalline tin oxides are detected for the produced powders. However, both of them show broad peaks around ~27° and ~53° in their diffraction patterns. This feature becomes more pronounced with increasing applied voltage, with a simultaneous vanishing of the

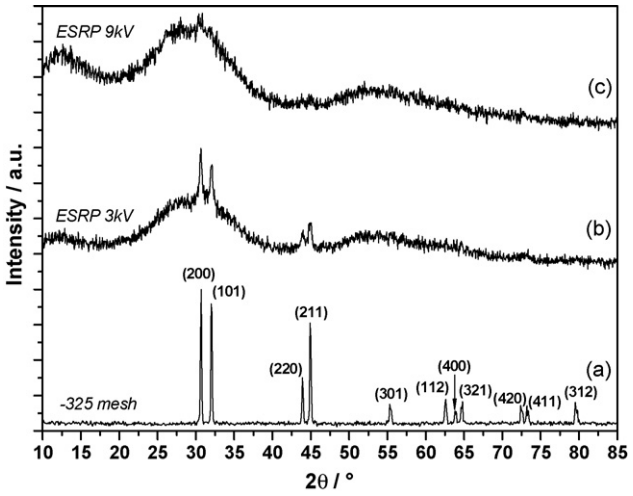

Fig. 2. XRD patterns of the materials obtained via ESRP with different voltages and commercial Sn powders. The intensities of the spectra are normalized.

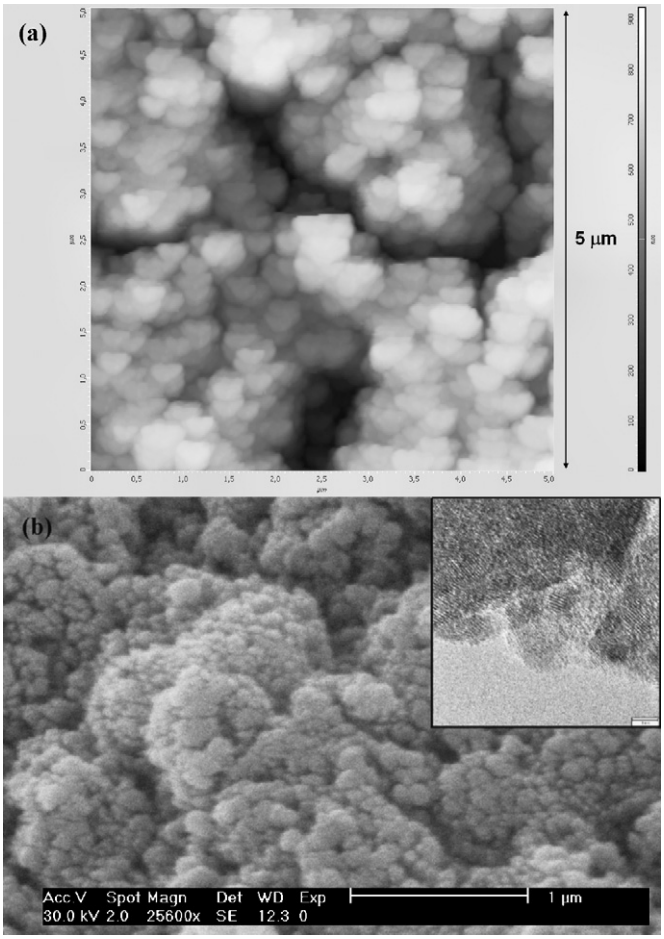

Fig. 3. Typical morphology for Sn powders synthesized via ESRP at 3 kV. AFM scan (5 μm × 5 μm) (a), and SEM micrograph (b). Au was sputtered onto the sample to allow clearer SEM imaging. The inset of (b) is a TEM micrograph, which shows the inner structure of the agglomerates; the scale bar in the inset is 3 nm.

sharp characteristic peaks. These broad diffractions are associated with SnO_2 contamination of the nanoparticles [19]. Reducing the size of the particles implies an enhanced surface reactivity, and it is not surprising that the materials have undergone oxidation during collection and manipulation. Interestingly, a similar diffraction pattern is displayed by composite Sn-based amorphous oxides [6,20], and the broad weak diffraction around 28° has been related to a distribution of Sn–Sn atomic distances in a glass matrix, as reported earlier by Idota et al. [6]. From these preliminary results, it can be concluded that increasing the voltage for the atomization, for a fixed flow rate, results in a higher tendency for oxidation and amorphization for the collected materials. Here, a nanocomposite material is expected, in which a crystalline tin phase is coexisting with an amorphous oxidic phase, as suggested by Fig. 2(b). A slight decrease in the average size of the crystallites can also contribute to the observed pattern of Fig. 2(c).

Conversely, powders produced via reductive precipitation by $NaBH_4$ show generally large surface areas, which cause easier contamination by oxidic and hydroxylic impurities [12]. Typical morphologies for the materials resulting from ESRP confirm that extended surface areas are expected for these products, and that they can play a determinant role in their electrochemical behaviour. Fig. 3 presents the typical morphology observed for the materials synthesized via ESRP at 3 kV.

As it can be seen from the pictures of Fig. 3(a) and (b), the powders are made up of continuous interconnections between the agglomerated clusters. An overall fluffy morphology is observed for the exposed surface of the materials, and no big bulky particles are detected. From the SEM picture (b) it is also noted that the agglomerated clusters have a rounded shape and their typical size is tens of nanometres. These agglomerates, on their turn, are further divided into crystalline domains with different sizes, surrounded by an amorphous phase, as it is shown by the TEM micrograph in the inset of Fig. 3(b).

The typical structure of the materials obtained via ESRP at 9 kV is presented in Fig. 4.

From Fig. 4(a) and (b) it is observed that the primary particles have sizes well below 10 nm. They are spherically shaped and show a homogeneous distribution, with an average size of about 3 nm. Crystalline domains are observed throughout the image. In the magnified inset of the picture, two Sn nanocrystals are clearly seen in a surrounding amorphous-like environment. Comparing this outcome with the XRD pattern of Fig. 2(c), it can be concluded that the primary particles are made up of one crystalline domain (i.e. a single crystallite). Hence, the presence of very small crystallites, combined with the oxide contamination of the particles, is responsible for the broad humps observed in the diffraction pattern. A nanocomposite material is therefore the result of the ESRP process under these experimental conditions. Sn nanocrystals of few nanometres are surrounded by an amorphous oxidic phase (i.e. SnO_x). As already mentioned, a Sn-based nanocomposite material is expected to enhance the stability during cycling.

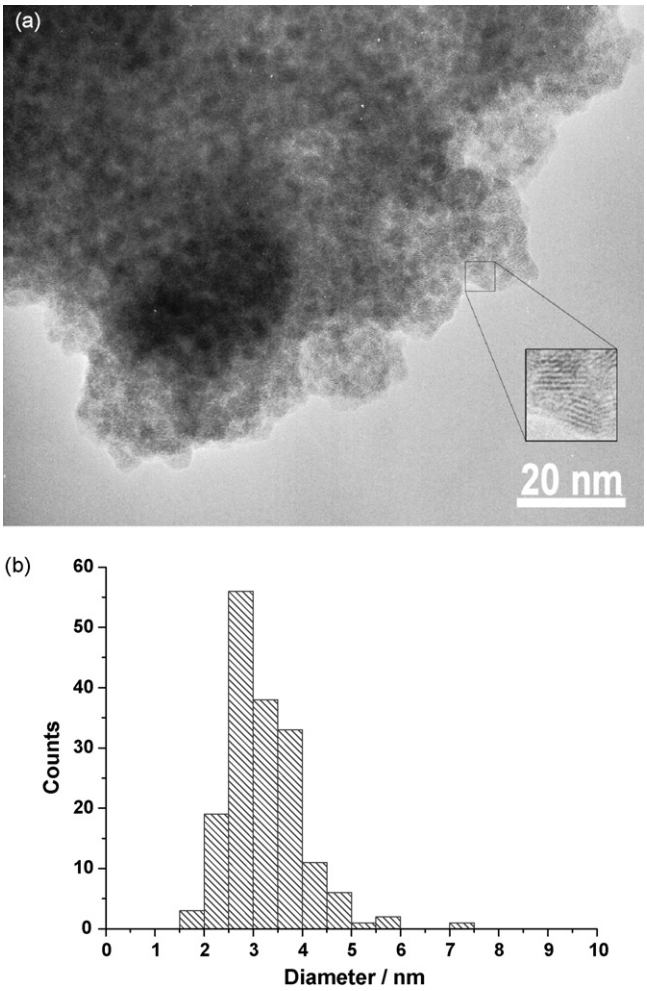

Fig. 4. TEM micrograph of the powders produced via ESRP at 9 kV (a). Size distribution for 170 measured particles (b).

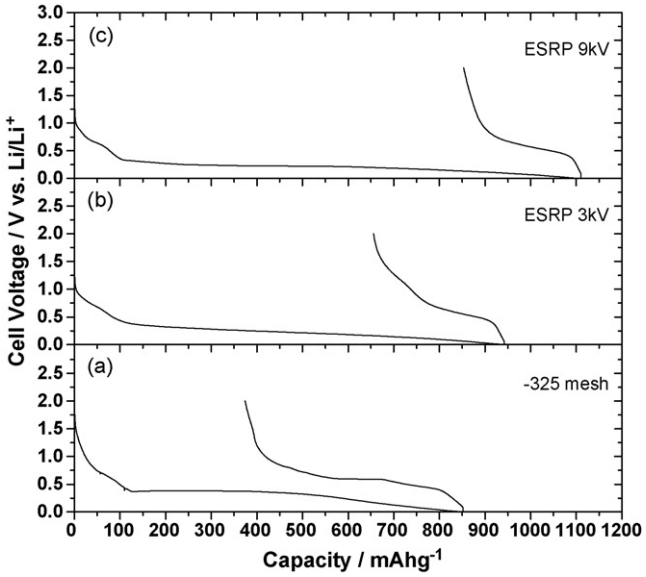

Fig. 5. Voltage profiles for the first cycle of discharge–charge at 113 mA g^{-1} between 0.0 and 2.0 V. Commercial powders (a), powders synthesized at 3 kV (b) and 9 kV (c).

In a composite SnO_x/Sn ($1 \le x \le 2$) electrode the electrochemical reactions of Li ions with the oxidic phase and metallic tin take place at different potentials during the first discharge, with the initial irreversible formation of Li_2O, according to the following reaction [21]:

$$2xLi^+ + 2xe^- + SnO_x \rightarrow xLi_2O + Sn \quad \text{with} \quad 1 \le x \le 2 \tag{1}$$

In general, it is known that most of the Li_2O is formed during the first cycle and that only a negligible amount of it can be recycled in the following cycles as the particle size is in the micrometer-scale range [21]. Then, Sn can reversibly react with Li according to the following reaction:

$$yLi^+ + ye^- + Sn \leftrightarrow Li_ySn \quad \text{with} \quad 0 < y \le 4.4 \tag{2}$$

The conversion reaction (1) is responsible for the formation of Sn clusters, which agglomerate and grow upon prolonged cycling, leading to loss of capacity [20].

Here Sn nanocrystals are created during the synthesis process, and they are in intimate contact with the Li_2O phase formed upon the first discharge. The presence of Li_2O in this case has a negative influence on the reversible capacity, but it can also have some beneficial effects. First of all, it acts as a buffering matrix alleviating the strain related to the volume changes. Secondly, it constitutes a fair ionic conductor, promoting the transport of Li ions to and from the Sn nanocrystals during discharge and charge. Finally, it could also lead to different mechanisms for Li storage, since Sn nanoparticles with size smaller than 10 nm could activate the transformation of Li_2O into Li^+, promoting a partial reversibility of the oxide [22].

Fig. 5 shows the first discharge–charge profiles for the electrodes containing the synthesized materials and the commercial powders.

The commercial powders show a discharge capacity of 852 mAh g^{-1}, which corresponds roughly to an uptake of 3.8 Li per unit Sn in the formed Li_ySn alloy. The main feature observed in Fig. 5(a) is the distinctive potential plateau around 0.4 V followed by a tail, indicating the formation of the Li-rich Sn alloy. A sloppy part at higher voltages is also observed for all the materials during the early stages of the discharge. No definite plateaus are detected for the produced materials, and the slight bending of the curves can be associated to the formation of the solid electrolyte interphase (SEI) at the initial stage of the lithiation process. It can be also noted that the capacity resulting from this part of the curve is comparable for all the materials. However, the final discharge capacities of Fig. 5(a)–(c) are clearly different. In the last case the amount of Li stored exceeds the theoretical value expected for the $Li_{4.4}Sn$ alloy, indicating extra storage probably due to surface effects and to the presence of amorphous oxide. The reversible capacity of the synthesized materials is negatively influenced by the presence of large surface areas, as it is observed in Fig. 5(b) and (c). Fig. 6 presents the evolution of the capacity upon subsequent cycling for the materials considered so far.

From Fig. 6 it is seen that the cycling behaviour of the commercial powders is completely different from those of the synthesized materials. Despite the higher reversible capacity shown during the first cycle (i.e. 478 mAh g^{-1}), a rapid capacity fading is observed after a few cycles, as is typically for micron-sized powders. The practical values are finally constant and are about 100 mAh g^{-1}. On the other hand, both materials synthesized via ESRP presented a higher Li uptake during the second discharge, which exceeded the poor values of the first charge (i.e. ~250–280 mAh g^{-1}). This behaviour, which is likely due to the presence of large surface areas, is observed for the first 5–6 cycles and it contributes to a substantial increase of the capacity up to ~450–465 mAh g^{-1}. This feature indicates that Sn-based nanocomposite powders can enhance the mechanical properties of the electrodes, which were not damaged by the volume changes of the first cycles. However, the capacities for both of them presented a moderate fading in the subsequent cycles. Their evolution does not show a substantial difference, apart from the fact that after 50 cycles the materials synthesized at 9 kV presented a certain tendency towards stabilization of the capacity. This could be due to a slight difference in the average size of the crystallites that resulted from the process at 3 and 9 kV, as suggested by the XRD patterns. In both cases, the final capacity is significantly higher than that of the commercial powders.

A different electrochemical test employed a lower current density for the first cycle (i.e. 23 mA g^{-1}) in order to favour a slower reaction kinetics and promote the diffusion of the Li ions. Besides, the voltage window for discharge and charge was reduced a little and fixed from 0.05 to 1.20 V, in order to provide a better combination of adequate capacity and cycleability. The voltage profiles of the materials during the first 10 cycles are shown in Fig. 7.

From Fig. 7(a) it is noted that the use of a reduced current density during the first cycle has a negative influence on the electrochemical behaviour of the commercial powders. The appearance of a hump at around 1.4 V causes an anomalous irreversible capacity,

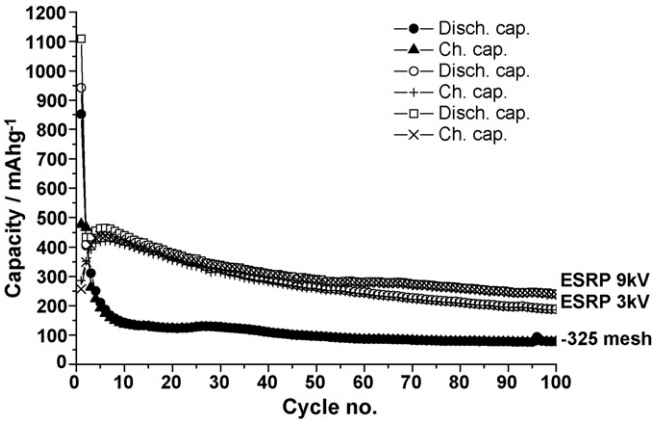

Fig. 6. Cycle performance of the materials tested between 0.0 and 2.0 V at 113 mA g^{-1}.

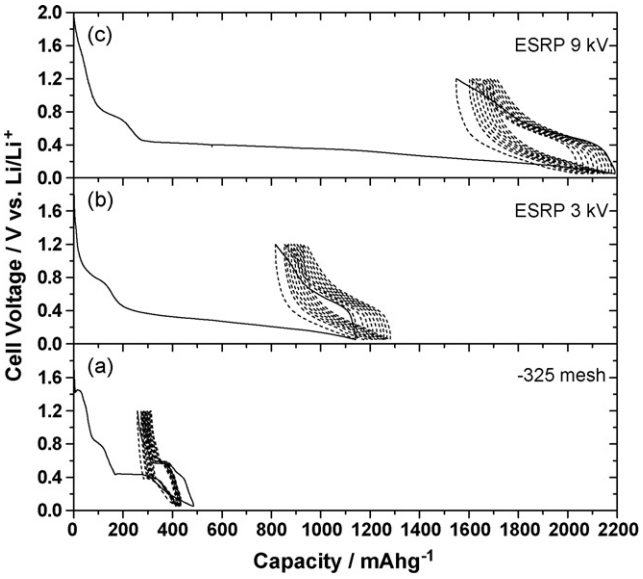

Fig. 7. Voltage profiles of the materials cycled between 0.05 and 1.20 V. Note that the first cycle (solid line) has been carried out at a reduced current density of 23 mA g^{-1} for all the materials. The following nine cycles performed at 113 mA g^{-1} (dotted lines) are also reported for further comparison.

which is associated to the catalytic decomposition of the electrolyte by the tin surface [8]. Moreover, such reaction is known to be influenced by the cycling rate, matching well with the previous observation. Indeed, the use of a higher cycling rate yielded no trace for this catalytic reaction (Fig. 5(a)). As the SEI layer grows thicker, due to the formation of a passivating film on the surface of the electrode, the transport of the Li ions through the interface is hindered. This is a possible explanation for the poorer capacities observed at the end of the first discharge and charge. The increase in the cycling rate during the subsequent cycles does not improve the cycling behaviour, and, after a further capacity fading, it yields only a minimal final capacity.

On the other hand, both materials synthesized via ESRP (Fig. 7(b) and (c)) present a huge increase of the discharge capacity, which exceed by far the theoretical value for Li–Sn alloy. Also in this case, no sharp plateaus are detected throughout their voltage profiles, indicating that the overall composition of the electrodes remains in a single phase region upon cycling, similarly as in a solid solution, where the potential depends on the state of charge. The observed reversibility for the cells is particularly poor during the first cycle (solid lines), and only a small part of the initial capacity is retained upon charge. It should be noted, however, that the recovered capacity has a practical value, still higher than the one observed for commercial Sn. The increase of the cycling rate during the second cycle has also in these cases the effect of further lowering the capacity, as better visualized in Fig. 8.

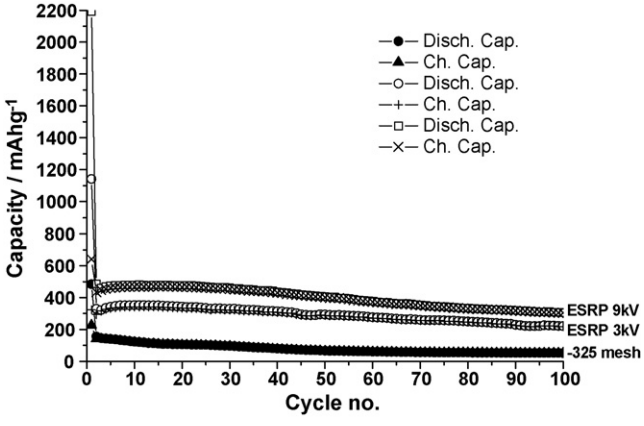

Fig. 8. Cycle performance of the materials tested between 0.05 and 1.20 V at a current density of 113 mA g^{-1}. Note that only the first cycle was performed at 23 mA g^{-1}.

It is clearly noticed that the electrodes containing the nanocomposite Sn/SnO_x powders can withstand prolonged cycling, retaining a certain capacity (i.e. ~220–300 mAh g^{-1}). In particular, their behaviour is stable over the first 20–30 cycles. The moderate capacity fading observed for these materials is not as severe as in the case of commercial powders.

4. Conclusions

Reductive precipitation by $NaBH_4$ was successfully coupled to electrospraying of Sn(II) chloride precursor for the synthesis of small Sn nanoparticles. Nanocomposite powders made up of Sn nanocrystals embedded in an amorphous oxidic SnO_x phase were the final products for this process. Increasing the applied voltage for the electrospraying resulted in an enhanced tendency towards the formation of monodispersed Sn crystallites. A comparison of the electrochemical behaviour of these materials with commercial Sn powders revealed that the powders resulting from this process yielded enhanced discharge capacities. Despite the high irreversible capacity observed during the first cycle, the powders showed a good stability in their cycling behaviour. We believe that a more careful manipulation of these materials under controlled atmosphere, together with suitable manufacturing of the electrodes can lead to improved cycle performances and limited irreversibilities.

Acknowledgements

The authors acknowledge the European Network of Excellence ALISTORE, the Dutch Ministry for Economic Affairs via SenterNovem and STW for funding the programme for nanomaterials syntheses. Marcel Bus, Ben Norder and Loïc Simonin are also gratefully acknowledged for their help, suggestions and collaboration.

References

[1] J.O. Besenhard, J. Yang, M. Winter, J. Power Sources 68 (1997) 87–90.
[2] M. Winter, J.O. Besenhard, M.E. Spahr, P. Novák, Adv. Mater. 10 (1998) 725–763.
[3] M. Winter, J.O. Besenhard, Electrochim. Acta 45 (1999) 31–50.
[4] J. Wang, D. Raistrick, R.A. Huggins, J. Electrochem. Soc. 133 (1986) 457–460.
[5] R.A. Huggins, J. Power Sources 81–82 (1999) 13–19.
[6] Y. Idota, T. Kubota, A. Matsufuji, Y. Maekawa, T. Miyasaka, Science 276 (1997) 1395–1397.
[7] J. Yang, M. Wachtler, M. Winter, J.O. Besenhard, Electrochem. Solid-State Lett. 2 (1999) 161–163.
[8] L.Y. Beaulieu, S.D. Beattie, T.D. Hatchard, J.R. Dahn, J. Electrochem. Soc. 150 (4) (2003) A419–A424.
[9] S. Naille, C.M. Ionica-Bousquet, F. Robert, F. Morato, P.-E. Lippens, J. Olivier-Fourcade, J. Power Sources 174 (2) (2007) 1091–1094.
[10] O. Mao, J.R. Dahn, J. Electrochem. Soc. 146 (2) (1999) 414–422.
[11] M. Wachtler, M. Winter, J.O. Besenhard, J. Power Sources 105 (2002) 151–160.
[12] A. Trifonova, M. Wachtler, M.R. Wagner, H. Schriettner, Ch. Mitterbauer, F. Hofer, K.C. Möller, M. Winter, J.O. Besenhard, Solid State Ionics 168 (2004) 51–59.
[13] Y. Wang, J.Y. Lee, T.C. Deivaraj, J. Electrochem. Soc. 151 (2004) A1804–A1809.
[14] M. Valvo, U. Lafont, L. Simonin, E.M. Kelder, J. Power Sources 174 (2007) 428–434.
[15] A.A. van Zomeren, E.M. Kelder, J.C.M. Marijnissen, J. Schoonman, J. Aerosol Sci. 25 (1994) 1229–1235.
[16] E.M. Kelder, O.C.J. Nijs, J. Schoonman, Solid State Ionics 68 (1994) 5–7.
[17] A. Jaworek, J. Mater. Sci. 42 (2007) 266–297.

[18] A. Jaworek, A. Krupa, J. Aerosol Sci. 30 (1999) 873–893.
[19] M. Noh, Y. Kim, M.G. Kim, H. Lee, H. Kim, Y. Kwon, Y. Lee, J. Cho, Chem. Mater. 17 (2005) 3320–3324.
[20] I.A. Courtney, W.R. McKinnon, J.R. Dahn, J. Electrochem. Soc. 146 (1999) 59–68.
[21] I.A. Courtney, J.R. Dahn, J. Electrochem. Soc. 144 (1997) 2045–2049.
[22] S.T. Chang, I.C. Leu, C.L. Liao, J.H. Yen, M.H. Hon, J. Mater. Chem. 14 (2004) 1821–1826.